

# Instance Separation Emerges from Inpainting

Steffen Wolf<sup>1</sup> Fred A. Hamprecht<sup>1</sup> Jan Funke<sup>2</sup>

## Abstract

Deep neural networks trained to inpaint partially occluded images show a deep understanding of image composition and have even been shown to remove objects from images convincingly. In this work, we investigate how this implicit knowledge of image composition can be leveraged for fully self-supervised instance separation. We propose a measure for the independence of two image regions given a fully self-supervised inpainting network and separate objects by maximizing this independence. We evaluate our method on two microscopy image datasets and show that it reaches similar segmentation performance to fully supervised methods.

## 1. Motivation

Recent inpainting neural networks demonstrate a remarkable ability to remove distortions in natural images (e.g., text overlays, watermarks, or pixel-wise independent noise) and are even able to entirely remove foreground objects (e.g., a flagpole as demonstrated [here](#)). Trained on large datasets, these networks learn the statistics that underlie images in a way that goes well beyond low level features. In this work, we aim to leverage those learnt statistics to distinguish individual objects in images from each other, without any form of supervision.

To intuitively understand how these statistics can be used, consider the following thought experiment. We train a high-capacity inpainting network on a very large corpus of natural images and imagine the following scenario: Given the image of a busy street with a region in the center masked out to inpaint, such a network will be able to continue inpainting cars that are partially visible. If, however, the masked-out region is large enough to contain entire objects, the provided context will be uninformative about their location, shape, and texture and will therefore not be able to recover those objects. In other words, the success of

<sup>1</sup>IWR/HCI, Heidelberg University, Germany <sup>2</sup>HHMI Janelia, Ashburn, VA. Correspondence to: Steffen Wolf <steffen.wolf@iwr.uni-heidelberg.de>.

Preliminary work.

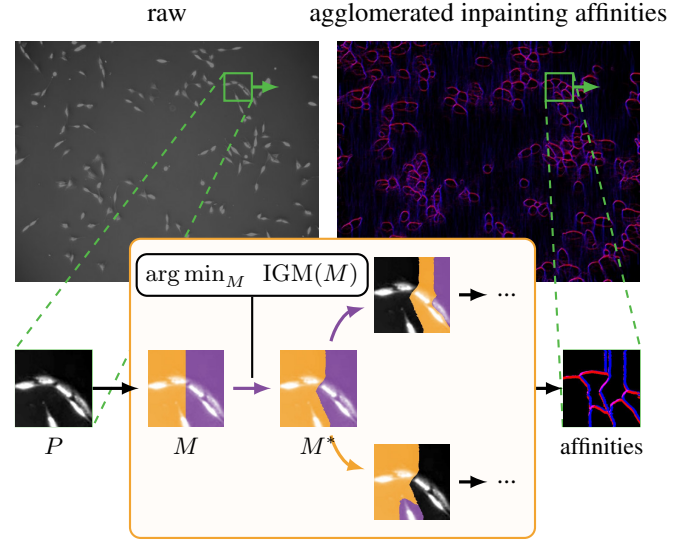


Figure 1: Extraction of instance separating affinities from an inpainting network. Given an image patch  $P$ , we optimize a set of pixels  $M$  (shown in purple) to minimize the *information gain measure*  $IGM$ , which is based on the predictions of a probabilistic inpainting network (see Section 2.2 and Fig. 2 for details). This optimization ensures that pixels in  $M^*$  provide minimal information about the intensity values of pixels in the complement  $\bar{M}^*$  (shown in orange). We apply this procedure recursively to  $M^*$  and  $\bar{M}^*$  to obtain a hierarchical segmentation of the image patch from which we extract affinities (shown in blue/red for x-/y-direction, respectively). These affinities are computed and averaged over a set of sliding image patches (green box) to obtain the final affinity estimates.

predicting masked out objects depends on the information about those object contained in the surrounding context.

Here, we propose to exploit the predictability of image regions given partial information to separate instances. We do so by maximizing the surprise of the inpainting network when trying to predict image content from one segment to another, or, equivalently, by minimizing the information gain between segments. This optimization can be carried out using only the implicit knowledge of inpainting networks about instances and thus gives rise to a self-

supervised instance separation.

In particular, we define an information gain measure between image segments that can be approximated efficiently given an inpainting network. We show that minimizing this measure, through a hierarchical optimization algorithm yields useful image decompositions. We represent those decompositions by *affinities*, *i.e.*, attractive or repulsive edges between pairs of pixels, which we average over a set of image patches in a sliding window fashion to obtain affinities for arbitrarily large images. An overview of this method is shown in Fig. 1. The resulting affinities require only minimal post-processing to obtain a segmentation. We apply our method to the challenging problem of cell segmentation in microscopy images, where we show that the unsupervised instance separation finds non-trivial splits and is competitive with supervised methods.

## 2. Self-Supervised Segmentation

In general, self-supervised segmentation is an under-constrained problem. What exactly constitutes a correct segmentation of an image depends not only on the application context (*e.g.*, segment all cells in a microscopy image), but also on a subjective level of detail (*e.g.*, segment nuclei and cell membrane individually). Without constraining assumptions or instructions, several different segmentations of the same image are plausible, leading to an intrinsic ambiguity. This ambiguity can be prominently observed as the inter-human variance for segmentation tasks where the concept of a segment is not precisely defined (see, *e.g.*, human generated segmentations of the BSD500 dataset for **fruits**, **fences**, or **flowers**)(Arbelaez et al., 2011).

In the case of supervised image segmentation, this ambiguity is resolved by a set of training object instances in the form of, *e.g.*, affinities, labeled images, bounding boxes, or polygons. For self-supervised segmentation, on the other hand, assumptions about what constitutes a segmentation have to fill in for the lack of training data.

Here, we propose to resolve this ambiguity by assuming that pixels of the same instance are more predictable from each other than across instances. We define the similarity between two pixels (and therefore the likelihood to be part of the same instance) as the information gained about the value of one pixel by observing the value of the other one. In the following we will derive this similarity from a measure of inpainting accuracy.

### 2.1. Self-supervised Inpainting

Let  $x_i$  be a random variable representing the intensity of pixel  $i \in \Omega$ , and  $x_M$  with  $M \subseteq \Omega$  a set of random variables  $\{x_i \mid i \in M\}$ . Probabilistic inpainting is equivalent to learning a parameterized function  $p_\theta(x_i|x_M)$ , *i.e.*,

the conditional distribution over intensities of pixel  $i$ , given known intensities of a partial observation  $M$ . The parameters  $\theta$  of the distribution  $p_\theta$  can be learned by maximizing the likelihood of a measurement  $x = x^*$ , or equivalently by minimizing the following negative log-likelihood:

$$\mathcal{L}_{\text{inpaint}}(\theta; M) = \sum_{i \notin M} -\log p_\theta(x_i = x_i^* | x_M = x_M^*) \quad (1)$$

It is worth noting that this loss formulation resembles the objective of probabilistic NOISE2VOID (Krull et al., 2019b), highlighting the close connection between inpainting and denoising. In the next subsection, we will derive a similar connection between inpainting (“predictability”) and instance separation (“affinity”).

### 2.2. Predictability is Affinity

Our central assumption is that the intensity value of a pixel in an instance is conditionally independent of all pixels outside the instance.

In other words, pixel values should be well predictable given the values of other pixels in the same instance (high affinity). Conversely, pixel values from other instances should provide *no additional* information (low affinity). More formally, let  $S = \{S_u \subseteq \Omega\}$  be a segmentation of  $\Omega$  (*i.e.*,  $\bigcup_u S_u = \Omega$  and  $\forall u \neq v : S_u \cap S_v = \emptyset$ ), and let  $S(i) \subseteq \Omega$  denote the segment containing pixel  $i$ . We assume that for the true instance segmentation  $S^*$

$$p(x_i | x_{\Omega \setminus \{i\}}) = p(x_i | x_{S^*(i) \setminus \{i\}}), \quad (2)$$

or, equivalently, that there is *no further* information gain provided by  $\Omega$  compared to  $S^*(i)$  for estimating the value of  $x_i$ . For general subsets  $M \subseteq \Omega$ , let  $\text{IG}(i|M)$  denote the additional information gained for estimating the value of  $x_i$  when observing  $\Omega$  compared to  $M$  alone, *i.e.*,

$$\text{IG}(i|M) = D_{\text{KL}}\left(p(x_i | x_{\Omega \setminus \{i\}}) \parallel p(x_i | x_{M \setminus \{i\}})\right), \quad (3)$$

where  $D_{\text{KL}}$  denotes the Kullback-Leibler divergence. In the following, we will use  $\text{IG}(i|M)$  as a measure of how much  $x_i$  depends on values *not* contained in  $M$ .

Considering our assumption stated in (2), a sensible objective to recover a single segment of the true segmentation  $S^*$  would be to minimize (3) with respect to  $M$ . In practice, however, it would be unreasonable to assume that even for a correct segment  $M$  the information gain for pixels in this set from pixels outside this set is exactly zero. In other words, dilating  $M$  would trivially decrease  $\text{IG}(i|M)$  until  $M = \Omega$ . Therefore, instead of minimizing (3) directly, we propose to minimize a symmetric information gain measure. Let  $\overline{M} = \Omega \setminus M$  be the complement of  $M$ . Recall that  $\text{IG}(i|M)$  measures the dependency of  $x_i$  on values in  $\overline{M}$ . We introduce a *relative* information gain that indicates

whether  $M$  or  $\bar{M}$  provide more information about the value of  $x_i$ :

$$\text{RIG}(i|M) = \text{IG}(i|M) - \text{IG}(i|\bar{M}). \quad (4)$$

The quality of a single segment  $M$  can now be assessed by the following symmetric information gain measure over all pixels  $i$ :

$$\text{IGM}(M) = \sum_{i \in M} \text{RIG}(i|M) + \sum_{i \in \bar{M}} \text{RIG}(i|\bar{M}) \quad (5)$$

$$= \sum_{i \in M} \text{RIG}(i|M) - \sum_{i \in \bar{M}} \text{RIG}(i|M). \quad (6)$$

### 2.3. Efficient Implementation

In its current form,  $\text{IGM}(M)$  requires evaluation of  $\text{IG}(i|M)$  for every pixel  $i \in \Omega$ . For each of these evaluations,  $p_\theta(x_i|\cdot)$  has to be computed two times (conditioned on  $M$  and  $\bar{M}$ ), which is too inefficient for a practical implementation.

To remedy this inefficiency, we make two approximations: First, we take advantage of convolutional neural network architectures that can inpaint an arbitrary set of pixels  $N$  for the same conditional (Liu et al., 2018):

$$\prod_{i \in N} p_\theta(x_i|M \setminus \{i\}) \approx \prod_{i \in N} p_\theta(x_i|M \setminus N) \quad (7)$$

A similar approximation technique was first proposed by Krull et al. (2019a) who argue that this approximation is error-free for convolutional neuronal networks, if all pixels in  $N$  are spaced further apart than the field of view of the network. In our experiments, we find that even much denser subsets can be chosen without significant impact. We will refer to  $\text{RIG}(i|M)$  using this approximation as  $\text{RIG}_N(i|M)$  in the following.

Second, due to the limited field of view of the inpainting network, pixels far away from the conditional set have to be estimated via a constant prior and the relative information gain can therefore be computed without evaluating the neural network. Similarly, the complement conditional contains all pixels in the field of view. This is exactly the denoising setup of NOISE2VOID (Krull et al., 2019a). Therefore, for low-noise-images one can directly approximate  $\text{IG}(i|\Omega) \approx 0$  and otherwise apply the NOISE2VOID as a preprocessing step to our method. Thus,  $\text{RIG}(i|M) \approx \text{const}$  for pixels far away from the boundary between  $M$  and  $\bar{M}$ .

In conclusion, limiting the computation of  $\text{IGM}$  to a specified region  $N$  close to the boundary combined with the

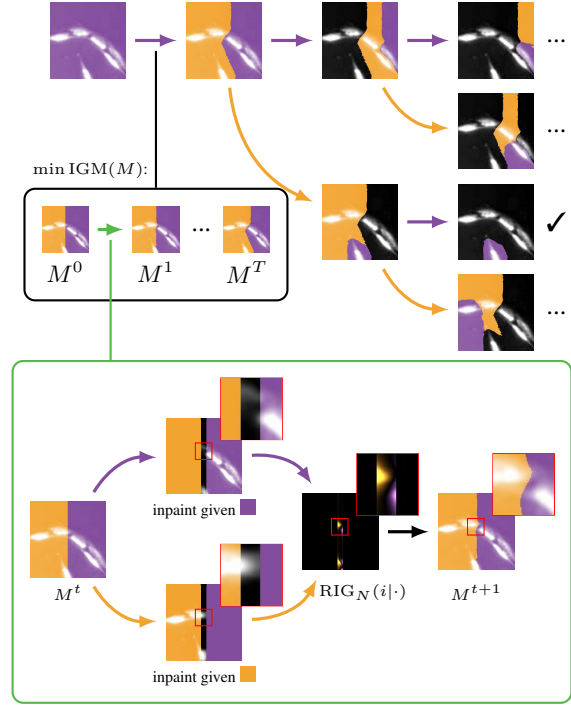


Figure 2: Details of the hierarchical segmentation of an image patch from an inpainting network. Given an image patch (top left), we recursively find optimal splits (shown in orange and purple) by evolving a randomly chosen horizontal or vertical split over  $T$  iterations (black box). For each step (illustrated in the green box), we evolve the boundary of the split by consulting a probabilistic inpainting network to predict the intensity of pixels in a region  $N$  around the boundary, once given only the information contained in  $M$  and once in its complement  $\bar{M}$ . We then measure the relative information gain  $\text{RIG}_N$  in the inpainting region to determine which component (orange or purple) provided more information about the pixels in  $N$  and reassign  $M$  accordingly.

approximate  $\text{RIG}_N$  leads to the following approximation:

$$\text{IGM}_N(M) = \sum_{i \in M \cap N} \text{RIG}_N(i|M) - \sum_{i \in \bar{M} \cap N} \text{RIG}_N(i|M) \quad (8)$$

$$\approx \text{IGM}(M) + \text{const} \quad (9)$$

### 2.4. Segmentation from Maximal Independent Regions

Although the approximation  $\text{IGM}_N$  introduced above reduces the computational burden of evaluating  $\text{IGM}$ , finding an optimal mask

$$M^* = \arg \min_M \text{IGM}_N(M) \quad (10)$$

still remains intractable in general due to the combinatorial number of possible masks. We propose to solve this optimization problem by following a greedy optimization strategy that generates a sequence of masks  $M^t$  for  $t \in \{0, \dots, T\}$  such that  $\text{IGM}_N(M^{t+1}) \leq \text{IGM}_N(M^t)$ , illustrated in Fig. 2.

To this end, we first separate  $\Omega$  into two equally sized components  $M^0$  and  $\overline{M}^0$  by randomly splitting them horizontally or vertically. We then evolve the boundary of the split by evaluating  $\text{RIG}_N(i|M^t)$  for all pixels  $i \in N$  in close proximity to the current boundary between  $M^t$  and  $\overline{M}^t$ . The sign of  $\text{RIG}_N(i|M^t)$  indicates whether  $M^t$  or  $\overline{M}^t$  provide more information about the pixel  $i$ . We update  $M$  accordingly, *i.e.*,

$$M^{t+1} = (M^t \setminus N) \cup \{i \in N \mid \text{RIG}_N(i|M^t) > 0\}, \quad (11)$$

which, by definition of (8), monotonically decreases  $\text{IGM}_N$ .

Finally, in order to obtain a decomposition of an image into arbitrarily many maximally independent regions, we apply the minimization recursively to already identified regions, *i.e.*, we repeat the optimization procedure described above on regions  $M^*$  and  $\overline{M}^*$ , until either  $M^*$  or  $\overline{M}^*$  are empty. Further implementation details on our neighborhood selection can be found in the appendix.

In order to extract affinities for a full image we compute maximally independent regions on a set of overlapping, sliding image patches and average their affinities. This procedure is illustrated in Fig. 1.

### 3. Experiments on Microscopy Image Instance Segmentation

Instance separation is of particular importance for the identification and tracking of individual cells in microscopy images, where cells frequently form densely packed clusters and thus pose a challenging segmentation problem (Ulman et al., 2017). In many cases, those cells are freely moving in a substrate and can thus be considered as many independent instances of the same kind, which makes them suitable for an inpainting based approach like the one we propose here and in particular for the independence assumption we made in (2). In the following, we will refer to the affinities extracted using the proposed method as INPAINTAFF.

#### 3.1. Cell Segmentation Benchmark Dataset

We evaluate INPAINTAFF on a subset of the ISBI Cell Segmentation Benchmark, which includes a diverse set of 2D microscopy videos covering a wide range of cell types and imaging quality.

In particular, we selected two datasets that contain cells

of irregular shape in close proximity for which instance separation is needed to obtain a correct segmentation: (1) HELA contains cervical cancer cells expressing H2b-GFP and (2) PANC contains pancreatic stem cells on a polystyrene substrate (see Fig. 6 for samples and the [CTC website](#) for further information about the datasets).

The PANC dataset arguably belongs to the more difficult datasets of the ISBI Cell Segmentation Benchmark (reflected in the comparatively low test scores on the challenge), which we attribute to two factors that are found in both HELA and PANC: First, they contain a large amount of touching cells with little boundary evidence, which renders a mere foreground segmentation ineffective for the detection of individual cells. Second, both datasets contain only little labeled training data (815 instances<sup>1</sup> for HELA and 514 for PANC in fully labeled frames), which challenges fully supervised segmentation approaches.

#### 3.2. Results

As argued earlier, completely unsupervised segmentation is an under-constrained problem. As such, INPAINTAFF alone is unlikely to give rise to a segmentation capturing the intuition of a human annotator. We recall that the main guiding principle for INPAINTAFF is predictability of pixel intensities. Depending on the distribution of cells in images used to train the inpainting network, this predictability might equally well apply to a background region around each cell. This effect is visible in both datasets (compare Fig. 6) and demonstrates that the method is agnostic about the intensity of pixels and merely clusters pixels that are mutually predictable.

Therefore, we investigate first how well INPAINTAFF separates instances. We then turn to the problem of instance segmentation, where we assume that at least a small amount of ground-truth labels is available to capture the notion of objects of interest—an assumption that arguably holds for any realistic application in practice, where an accurate segmentation is required.

We report results using the ISBI Cell Segmentation Benchmark segmentation accuracy (SEG score), a metric that is based on the Jaccard similarity index and measures average IoU of all segments that overlap at least 50% with the ground truth (further details are given on the [challenge website](#)). The detection score is the percentage of matches that surpass a set IoU threshold.

**Instance Separation** We investigate how well INPAINTAFF separates instances, assuming that an accurate foreground segmentation is already available. For that,

<sup>1</sup>HELA has 571 additional instances, in partially labeled frames which can not trivially be used to train neural networks.



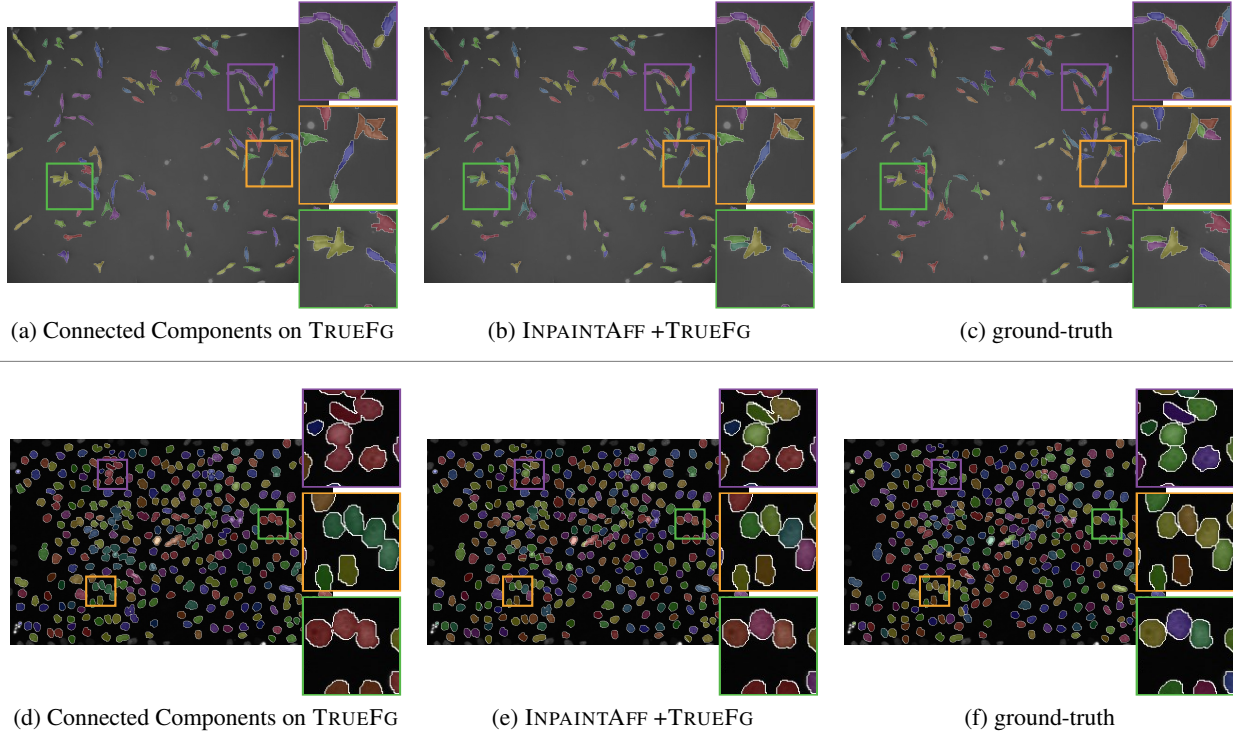


Figure 3: Instance separation results assuming an accurate foreground detection TRUEFG on the PANC dataset (top row) and the HELA dataset (bottom row). A foreground detection alone is not sufficient to segment touching cells (a, d). INPAINTAFF extracted from an inpainting network find non-trivial splits between instances (b, e).

Method		HELA	PANC
Connected Components on TRUEFG		0.785	0.748
INPAINTAFF + TRUEFG		0.858	0.914
INPAINTAFF + FGNET50		0.766	0.666
HIT-CN*	MU-Lux-CZ*	0.919	0.715
FR-Ro-GE*	CVUT-CZ*	0.903	0.682
PURD-US*	HD-Hau-GE*	0.902	0.665

Table 1: Segmentation scores assuming an accurate foreground detection TRUEFG and FGNET50 (trained with 52/49 labeled instances for HELA/PANC). For reference, we include the official challenge scores of supervised methods on the same datasets (marked with a star), which have been trained on more labeled instances and evaluated on a different testing dataset than our method.

we use the ground-truth segmentation provided in the datasets and convert it into a binary foreground segmentation TRUEFG, while connecting all segments separated by a one pixel wide gap.

As we show in Table 1 (and qualitatively in Fig. 3), TRUEFG alone is not sufficient to achieve an accurate instance segmentation, due to merges of cells in close prox-

imity. Separating those cells using INPAINTAFF, however, results in an almost perfect instance segmentation, in the case of PANC even significantly exceeding the scores of the best performing methods (albeit on different testing data and constrained to the ground-truth foreground). Those results suggest that (1) INPAINTAFF is accurately separating instances, and (2) a foreground segmentation is necessary and sufficient to constrain the boundaries of found objects to obtain a competitive segmentation.

### Instance Segmentation from Foreground Prediction

Since a foreground segmentation is crucial to capture the application specific notion of what constitutes an object, we next investigate the segmentation accuracy of our method when combined with a foreground prediction network trained on few instances only, which we will refer to as FGNET (details in Section 3.3). We train FGNET on varying amounts of labeled instances to predict a binary foreground mask and use this prediction in combination with our INPAINTAFF to obtain an instance segmentation. As a baseline, we also train a second network AFFNET to predict affinities directly from the same labeled instances used to train the foreground network.

The segmentation scores for either approach on the test

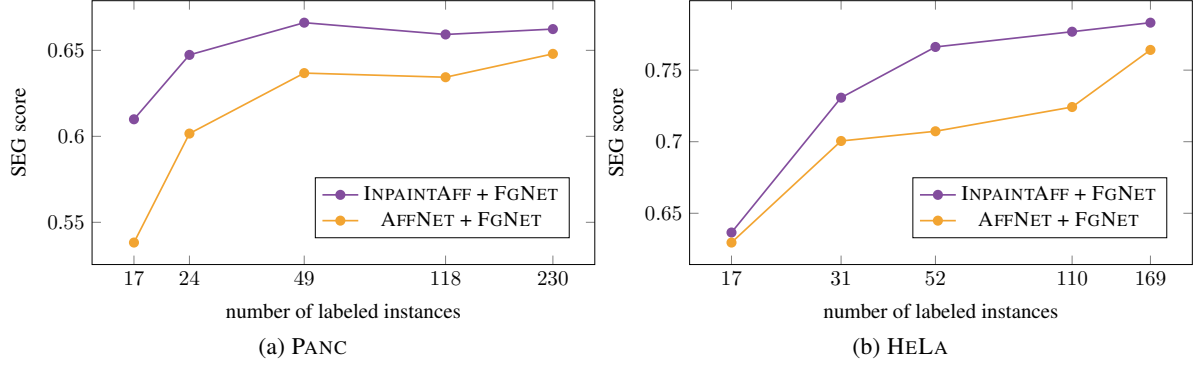


Figure 4: Segmentation score on the test data of datasets PANC and HELA, for varying amounts of labeled instances used to train FGNET and AFFNET.

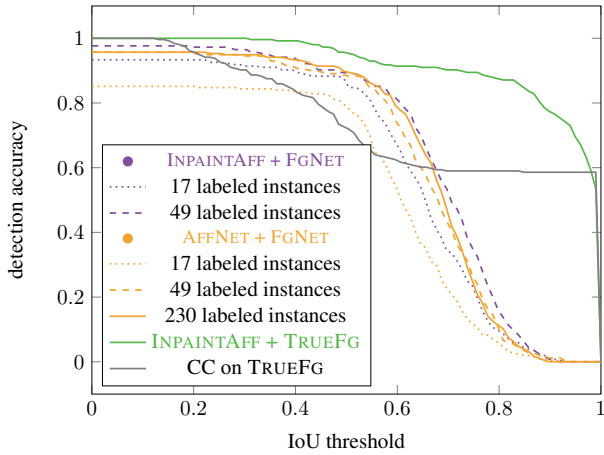


Figure 5: Detection accuracy over different IoU thresholds on PANC. Over a large range of IoU thresholds, INPAINTAFF in combination with a foreground network FGNET trained on 49 labeled instances has a higher detection accuracy than the fully supervised method AFFNET trained on 230 labeled instances.

dataset are shown in Fig. 4, for varying amounts of labeled instances used for training. Remarkably, INPAINTAFF consistently outperform trained affinities in terms of the SEG score. This effect is most visible in dataset PANC, where cells tend to cluster more compactly and the separation of individual cells is therefore more challenging. In particular, INPAINTAFF on this dataset in combination with FGNET trained on as few as 24 labeled cells produce a segmentation that outperforms the fully supervised AFFNET using one order of magnitude more training data. As shown in Fig. 5, this observation also holds in terms of the detection score over varying IoU thresholds. Furthermore, on the PANC datasets the obtained segmentation score using only around 50 labeled instances for the foreground prediction together with unsupervised affinities is on par with the third leading submissions to the ISBI Cell Segmentation

Benchmark, which have been trained on 514 instances (albeit evaluated on a different testing dataset than used here).

### 3.3. Experiment Details

**Training and Testing Split** Since INPAINTAFF requires a considerable amount of computational resources (see discussion in Section 5) a direct evaluation on the CTC servers on the official testing data is not possible. Therefore, we split the publicly available data for each dataset into a train and testing dataset, each containing one video of sparsely labeled cells. Further details can be found in the appendix.

**Model Architectures** For the inpainting network underlying INPAINTAFF, we use a downscaled version of the architecture proposed by Liu et al. (2018), *i.e.*, a U-NET architecture with a depth of four resulting in five levels with 64, 128, 256, 512, and 512 feature maps, each. We train the network for 1M iterations using the ADAM optimizer and the loss proposed by Liu et al. (2018) that is comprised of a perceptual, style, total variation and reconstruction loss.

FGNET is a PIX2PIX network (Zhu et al., 2017; Isola et al., 2017) with a depth of six layers, containing 64 initial features maps, trained using ADAM to minimize a binary cross-entropy loss (Kingma & Ba, 2014).

Since we use the MUTEXWATERSHED to post-process affinity predictions, we use the same training procedure proposed by Wolf et al. (2018) for AFFNET (PIX2PIX architecture). In particular, we also use the Sørensen-Dice coefficient (Dice, 1945; Sørensen, 1948) loss and the same affinity neighborhood (12 distances, up to 27 pixels).

**Affinity-Based Segmentation** We use the MUTEXWATERSHED to derive a segmentation from affinities (Wolf et al., 2018), where we introduce a single parameter  $\alpha$  to control for over- and undersegmentation by multiplying all long range affinities (that are used to split) with  $\alpha$ . The op-

timal  $\alpha$  for each evaluated method was determined on the validation dataset. For further details can be found in the appendix.

## 4. Related Work

While classical patch-based inpainting methods such as (Drori et al., 2003; Sun et al., 2005; Barnes et al., 2009) synthesize high quality images, they fundamentally cannot make semantically aware decisions for intensity predictions. Deep inpainting networks, on the other hand, trained on large corpuses of data are known to develop an intrinsic understanding of images (Larsson et al., 2017), which raises the question what aspects are captured by these networks. The usefulness of these inpainting models for image segmentation was shown by Pathak et al. (2016), who demonstrate that features extracted from a trained inpainting network capture appearance and semantics of visual structures aiding in the pre-training of classification, detection, and segmentation tasks. Extending inpainting networks that directly minimize the reconstruction error (Xie et al., 2012; Köhler et al., 2014) with texture and structure aware loss, such as multi-scale neural patch synthesis (Yang et al., 2017) or Structure-aware Appearance Flow (Ren et al., 2019) leads to high-fidelity images and prediction and modeling of higher order relations

In parallel, specialized architectures and convolutions have been developed that make it possible to realistically inpaint arbitrary masks (Liu et al., 2018; Yu et al., 2019).

In this work, we use the network architecture and loss proposed by Liu et al. (2018) which is designed to inpaint arbitrary masks and is trained with an additional style component loss. Since we leverage the network’s learned distribution by measuring information gain between image patches, we intentionally avoid networks trained with an additional GAN loss (Nazeri et al., 2019; Chen et al., 2018; Zeng et al., 2019). Although GANs produce extremely realistic looking images, they are prone to mode collapse that affects our estimate of information gain.

More generally, inpainting falls under the broader category of unsupervised prediction of left-out data, also known as *self-supervised* learning (de Sa, 1994). This includes tasks such as image colorization (Zhang et al., 2016; Larsson et al., 2016), co-occurrence (Isola et al., 2015), predicting permutations (Santa Cruz et al., 2017), and denoising (Krull et al., 2019a). These methods are highly effective at extracting robust features for further transfer learning (Zhang et al., 2017) and image embeddings (Trinh et al., 2019) and can be considered a proxy task for developing a semantic understanding (Larsson et al., 2017).

In some cases, the self-supervised task can be used as a free supervisory signal that directly translates to classically

supervised tasks. For example, object tracking emerges from video colorization (Vondrick et al., 2018) (which inspired our title) or through obeying cycle-consistency in time (Wang et al., 2019). When provided with background images and images with objects, Ostyakov et al. (2018) learn to segment by predicting masks and paste patches from the object domain onto the background domain constrained by an adversarial and a cycle consistency loss.

Our work uses the statistical properties of instances to derive a method for separating instances, which closely relates to other self-supervised segmentation approaches that utilize different properties to identify objects. Burgess et al. (2019) utilize compressibility, in a compositional generative model, where image regions are reconstructed through a low dimensional bottleneck. They show that their model is capable of discovering useful decompositions of scenes by identifying segments that can be represented in a common format. Another approach by Chen et al. (2019) learns to find masks of objects by learning to replace the masked content content that corresponds with altering the masked objects properties (e.g. altering the color of flowers).

## 5. Discussion

It remains an open question as to how far completely unsupervised segmentation based on image statistics alone will find real world applications. As we already observed on the segmentation of cells in microscopy images studied here, an experimentalist’s intention of what constitutes a good cell segmentation does not necessarily match the clustering of pixels based on information content. Only at least partially supervised methods with application specific losses can ultimately produce predictions tailored to a specific application, provided enough labeled training data is available. We see the contribution of this work therefore primarily as an aid to supervised methods, especially in scenarios in which labeled training data is scarce. As our experiments demonstrate, INPAINTAFF allow practitioners to obtain competitive segmentations from very few labeled instances. Given the high rate and diversity of microscopy images acquired in the life sciences, self-supervised segmentation has the potential to significantly reduce the amount of human interaction needed. Our work shows that in this domain the inherent knowledge captured by inpainting networks provides competitive performance with very few labeled instances.

A limitation of the method proposed here is the runtime: INPAINTAFF requires around 48h to process a 700x1100 image on a single GPU. Although inference can be trivially parallelized, the current implementation might be prohibitively slow for many applications. Increasing the efficiency of the inference by, e.g., training networks directly on IGM, will be subject of future work.



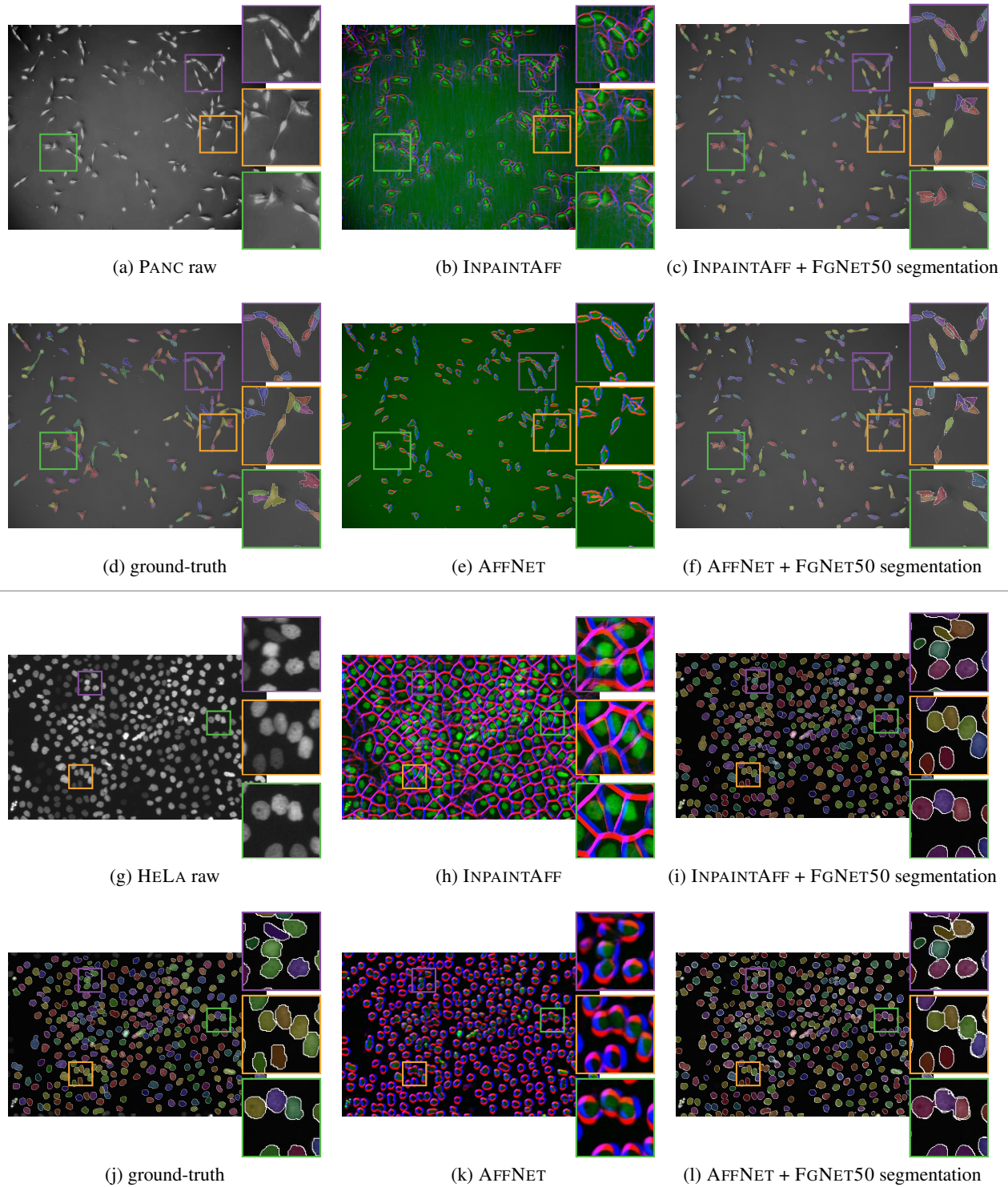


Figure 6: Sample test images of PANC (top) and HELA (bottom). Affinities (middle column) are shown as blue/red for x-/y-direction, respectively.



## References

- Arbelaez, P., Maire, M., Fowlkes, C., and Malik, J. Contour detection and hierarchical image segmentation. *IEEE Trans. Pattern Anal. Mach. Intell.*, 33(5):898–916, May 2011. ISSN 0162-8828. doi: 10.1109/TPAMI.2010.161. [2](#)
- Barnes, C., Shechtman, E., Finkelstein, A., and Goldman, D. B. Patchmatch: A randomized correspondence algorithm for structural image editing. In *ACM Transactions on Graphics (ToG)*, volume 28, pp. 24. ACM, 2009. [7](#)
- Burgess, C. P., Matthey, L., Watters, N., Kabra, R., Higgins, I., Botvinick, M., and Lerchner, A. Monet: Unsupervised scene decomposition and representation. *arXiv preprint arXiv:1901.11390*, 2019. [7](#)
- Chen, M., Artières, T., and Denoyer, L. Unsupervised object segmentation by redrawing. In *Advances in Neural Information Processing Systems*, pp. 12705–12716, 2019. [7](#)
- Chen, Z., Nie, S., Wu, T., and Healey, C. G. High resolution face completion with multiple controllable attributes via fully end-to-end progressive generative adversarial networks. *arXiv preprint arXiv:1801.07632*, 2018. [7](#)
- de Sa, V. R. Learning classification with unlabeled data. In *Advances in neural information processing systems*, pp. 112–119, 1994. [7](#)
- Dice, L. R. Measures of the amount of ecologic association between species. *Ecology*, 26(3):297–302, 1945. [6](#)
- Drori, I., Cohen-Or, D., and Yeshurun, H. Fragment-based image completion. In *ACM SIGGRAPH*, pp. 303–312. 2003. [7](#)
- Isola, P., Zoran, D., Krishnan, D., and Adelson, E. H. Learning visual groups from co-occurrences in space and time. *arXiv preprint arXiv:1511.06811*, 2015. [7](#)
- Isola, P., Zhu, J.-Y., Zhou, T., and Efros, A. A. Image-to-image translation with conditional adversarial networks. In *Proceedings of the IEEE conference on computer vision and pattern recognition*, pp. 1125–1134, 2017. [6](#)
- Kingma, D. P. and Ba, J. Adam: A method for stochastic optimization. *arXiv preprint arXiv:1412.6980*, 2014. [6](#)
- Köhler, R., Schuler, C., Schölkopf, B., and Harmeling, S. Mask-specific inpainting with deep neural networks. In *German Conference on Pattern Recognition*, pp. 523–534. Springer, 2014. [7](#)
- Krull, A., Buchholz, T.-O., and Jug, F. Noise2void-learning denoising from single noisy images. In *Proceedings of the IEEE Conference on Computer Vision and Pattern Recognition*, pp. 2129–2137, 2019a. [3](#), [7](#)
- Krull, A., Vicar, T., and Jug, F. Probabilistic noise2void: Unsupervised content-aware denoising. *arXiv preprint arXiv:1906.00651*, 2019b. [2](#)
- Larsson, G., Maire, M., and Shakhnarovich, G. Learning representations for automatic colorization. In *European Conference on Computer Vision*, pp. 577–593. Springer, 2016. [7](#)
- Larsson, G., Maire, M., and Shakhnarovich, G. Colorization as a proxy task for visual understanding. In *Proceedings of the IEEE Conference on Computer Vision and Pattern Recognition*, pp. 6874–6883, 2017. [7](#)
- Liu, G., Reda, F. A., Shih, K. J., Wang, T.-C., Tao, A., and Catanzaro, B. Image inpainting for irregular holes using partial convolutions. In *The European Conference on Computer Vision (ECCV)*, 2018. [3](#), [6](#), [7](#)
- Nazeri, K., Ng, E., Joseph, T., Qureshi, F. Z., and Ebrahimi, M. Edgeconnect: Generative image inpainting with adversarial edge learning. *arXiv preprint arXiv:1901.00212*, 2019. [7](#)
- Ostypakov, P., Suvorov, R., Logacheva, E., Khomenko, O., and Nikolenko, S. I. Seigan: Towards compositional image generation by simultaneously learning to segment, enhance, and inpaint. *arXiv preprint arXiv:1811.07630*, 2018. [7](#)
- Pathak, D., Krahenbuhl, P., Donahue, J., Darrell, T., and Efros, A. A. Context encoders: Feature learning by inpainting. In *Proceedings of the IEEE conference on computer vision and pattern recognition*, pp. 2536–2544, 2016. [7](#)
- Ren, Y., Yu, X., Zhang, R., Li, T. H., Liu, S., and Li, G. Structureflow: Image inpainting via structure-aware appearance flow. In *Proceedings of the IEEE International Conference on Computer Vision*, pp. 181–190, 2019. [7](#)
- Santa Cruz, R., Fernando, B., Cherian, A., and Gould, S. DeepPermNet: visual permutation learning. In *Proceedings of the IEEE Conference on Computer Vision and Pattern Recognition*, pp. 3949–3957, 2017. [7](#)
- Sørensen, T. A method of establishing groups of equal amplitude in plant sociology based on similarity of species and its application to analyses of the vegetation on danish commons. *Biol. Skr.*, 5:1–34, 1948. [6](#)
- Sun, J., Yuan, L., Jia, J., and Shum, H.-Y. Image completion with structure propagation. In *ACM SIGGRAPH*, pp. 861–868. 2005. [7](#)
- Trinh, T. H., Luong, M.-T., and Le, Q. V. Selfie: Self-supervised pretraining for image embedding. *arXiv preprint arXiv:1906.02940*, 2019. [7](#)

- Ulman, V., Maška, M., Magnusson, K. E., Ronneberger, O., Haubold, C., Harder, N., Matula, P., Matula, P., Svoboda, D., Radojevic, M., et al. An objective comparison of cell-tracking algorithms. *Nature methods*, 14(12): 1141, 2017. 4
- Vondrick, C., Shrivastava, A., Fathi, A., Guadarrama, S., and Murphy, K. Tracking emerges by colorizing videos. In *Proceedings of the European Conference on Computer Vision (ECCV)*, pp. 391–408, 2018. 7
- Wang, X., Jabri, A., and Efros, A. A. Learning correspondence from the cycle-consistency of time. In *Proceedings of the IEEE Conference on Computer Vision and Pattern Recognition*, pp. 2566–2576, 2019. 7
- Wolf, S., Pape, C., Bailoni, A., Rahaman, N., Kreshuk, A., Kothe, U., and Hamprecht, F. The mutex watershed: efficient, parameter-free image partitioning. In *Proceedings of the European Conference on Computer Vision (ECCV)*, pp. 546–562, 2018. 6
- Xie, J., Xu, L., and Chen, E. Image denoising and inpainting with deep neural networks. In *Advances in neural information processing systems*, pp. 341–349, 2012. 7
- Yang, C., Lu, X., Lin, Z., Shechtman, E., Wang, O., and Li, H. High-resolution image inpainting using multi-scale neural patch synthesis. In *Proceedings of the IEEE Conference on Computer Vision and Pattern Recognition*, pp. 6721–6729, 2017. 7
- Yu, J., Lin, Z., Yang, J., Shen, X., Lu, X., and Huang, T. S. Free-form image inpainting with gated convolution. In *Proceedings of the IEEE International Conference on Computer Vision*, pp. 4471–4480, 2019. 7
- Zeng, Y., Fu, J., Chao, H., and Guo, B. Learning pyramid-context encoder network for high-quality image inpainting. In *Proceedings of the IEEE conference on computer vision and pattern recognition*, pp. 1486–1494, 2019. 7
- Zhang, R., Isola, P., and Efros, A. A. Colorful image colorization. In *European conference on computer vision*, pp. 649–666. Springer, 2016. 7
- Zhang, R., Isola, P., and Efros, A. A. Split-brain autoencoders: Unsupervised learning by cross-channel prediction. In *Proceedings of the IEEE Conference on Computer Vision and Pattern Recognition*, pp. 1058–1067, 2017. 7
- Zhu, J.-Y., Park, T., Isola, P., and Efros, A. A. Unpaired image-to-image translation using cycle-consistent adversarial networks. In *Proceedings of the IEEE international conference on computer vision*, pp. 2223–2232, 2017. 6

## A. Neighborhood Selection and Inference:

As discussed, the updates of the equation (11) can be limited to  $N$ , a set of pixels close to the boundary of  $M$  and  $\overline{M}$ . Formally, let  $\text{FOV}(i, d)$  be the set of all pixels closer to pixel  $i$  than the max distance  $d$ . Then

$$N(M, d) = \left\{ i \in \Omega \mid \text{FOV}(i, d) \cap \overline{M} \neq \emptyset \text{ and } \right. \quad (12)$$

$$\left. \text{FOV}(i, d) \cap M \neq \emptyset \right\} \quad (13)$$

Empirically, we find that decreasing  $d$  over time aids the regions to converge. In our experiments, we use a constant  $d$  for the first half of the updates and then decrease it linearly. Additionally, we find that smoother boundaries can be achieved by interleaving updates with  $d = 1$  every second iteration and smoothing the reconstruction error over neighboring pixels. For the smoothing, we convolve the reconstruction error with gaussian kernels with  $\sigma \in [0.1, 1, 5, 10]$  and add them to the pixel-wise reconstruction error.

## B. Train/Test Split of CTC

Each dataset of the **Cell Tracking Challenge** contains two training (labeled  $t01$  and  $t02$ ) and two test videos. Since our inference method requires a considerable amount of computational resources, a direct evaluation on the CTC servers on the official testing data is not possible. Therefore, we split the publicly available data for each dataset into a train and testing dataset.

For the PANC (*PhC-C2DL-PSC*) dataset we train on frame 182 of video  $t02$ , validate on frame 25 of  $t02$  and test on frames [98, 122] of video  $t01$ . This uses all 4 available labeled frames of the dataset.

For the HE<sub>LA</sub> (*Fluo-N2DL-HeLa*) dataset we train on frames [13, 52] of video  $t01$ , validate on frame 76 of  $t01$  and test on all (even partially labeled) frames [23, 35, 36, 67, 75, 78, 79, 87] of video  $t02$ .

The training sets with a reduced number of instances were generated by first, using a random subset of labeled frames and then cropping the training images spatially. We alternate between halving the image size in x and y-direction, taking away from both sides, thus keeping the center constant.

## C. Affinity-Based Segmentation

We derive a segmentation from affinities  $\text{aff}$  using the **MUTEXWATERSHED** on a XY-plane neighborhood graph with local attractive edges  $[-1, 0], [0, -1]$  and sparse repulsive edges:  $[-9, 0], [0, -9], [-9, -9], [9, -9], [-9, -4], [-4, -9], [4, -9], [9, -4], [-27, 0], [0, -27]$ .

The graph weights for the local attractive edges are equivalent to the affinities, and the costs of the repulsive edges are the  $\alpha$ -weighted inverted affinities  $\alpha(1 - \text{aff})$ .